Available online at www.sciencedirect.com
ScienceDirect
Catalysis Today 136 (2008) 249–257
CATALYSIS TODAY
www.elsevier.com/locate/cattod

The micro-reactor testing of catalysts and fuel delivery apparatuses for diesel autothermal reforming

Inyong Kang [a], Sangho Yoon [a], Gyujong Bae [a], Jung Hyun Kim [a], Joongmyeon Bae [a,*], Daehoon Lee [b], Younghoon Song [b]

[a] *Department of Mechanical Engineering, Korea Institute of Science and Technology (KAIST), 335 Gwahangno, Yuseong-gu, Daejeon 305-701, Republic of Korea*
[b] *Environmental System Research Center, Korea Institute of Machinery & Materials (KIMM), 171 Jang-dong, Yuseong-gu, Daejeon 305-343, Republic of Korea*

Available online 3 March 2008

Abstract

This study investigated two factors affecting the performance of diesel autothermal reforming (ATR): the reforming activity of selected catalysts and the effect of devised fuel delivery apparatuses. When fluorite and perovskite-structured ceramic materials were used as substrates, H_2 yields were higher than when an inert Al_2O_3 substrate was used at 700–800 °C. Gadolinium (Gd)-doped CeO_2 (CGO) had the highest H_2 production rate in the selected substrates. Platinum (Pt) showed better performance than rhodium (Rh) and ruthenium (Ru) when CGO was used as the substrate. Although the nickel (Ni)-added Pt catalyst (Pt–Ni) showed high H_2 yield, carbon deposition over this catalyst was more severe than with Pt. Oxygen ion (O^{2-}) vacancies generated by Gd dopants can enhance the reforming activity of CeO_2. When using a microchannel catalyst bed, the performance degradation at high gas flowrates can be compared to a packed catalyst bed of pellet type. For effective fuel delivery, we have introduced an ultrasonic injector (UI) and a plasma injector (PI). The UI-reforming showed greater long-term stability than non-UI reforming because the generation of carbon precursors was suppressed. On the other hand, the PI-reformer had low conversion efficiency, although it had high H_2 selectivity.

Keywords: Diesel; Autothermal reforming (ATR); Catalysts; Microchannel; Ultrasonic injector (UI); Plasma injector (PI)

1. Introduction

A hydrogen infrastructure is required for the commercialization of fuel cells. Although developed countries have tried to construct an infrastructure, it is still far from commercialization. Fuel reforming technology is a very practical short-term alternative to supply hydrogen [1]. Fuel reforming chemically extracts hydrogen from hydrocarbon fuels, such as natural gas (NG), liquefied petroleum gas (LPG), gasoline, and diesel. Heterogeneous reactions with solid catalysts are generally used for effective hydrogen production in heavier hydrocarbon reforming [2].

There are three types of fuel reforming, steam reforming (SR), partial oxidation (POX), and autothermal reforming (ATR) [3–6]. SR is very mature technology which uses fuel and water as the reactants. Steam reformers, however, have several disadvantages in their application in fuel cell systems. They are limited by heat transfer because of the severe endothermicity of the reaction [7]. Its slow response behavior makes SR more suitable for plant-size reactors than mobile and transportable applications. In addition, SR has low conversion efficiency for heavier hydrocarbons such as diesel [8]. On the other hand, POX and ATR which use oxygen as a reactant have fast oxidation reactions [9]. They are driven by internally self-generated heat energy from the oxidation process. Therefore, compact POX and ATR reactors can be constructed [10]. They have high conversion rates for heavier hydrocarbons due to effective hydrocracking at the high temperatures of the oxidation process. The high operating temperature of POX and ATR sometimes leads to deactivation of the catalyst due to catalyst sintering causing difficulty in selecting materials for catalysts and reactors. In spite of these disadvantages, ATR is

* Corresponding author. Tel.: +82 42 869 3085; fax: +82 42 869 8207.
E-mail address: jmbae@kaist.ac.kr (J. Bae).

0920-5861/$ – see front matter © 2008 Elsevier B.V. All rights reserved.
doi:10.1016/j.cattod.2008.01.012

preferred over POX. It is because POX has high possibility of coke formation in absence of water. Because ATR uses both oxygen (or air) and water as reactants, exothermic POX and endothermic SR occur simultaneously in the ATR reactor [9,11]. ATR has a lower operating temperature than POX. Additionally, H_2O plays a key role in suppressing carbon deposition [8,12] and producing more H_2 by the water gas shift (WGS) reaction [9]. In these respects, ATR technology was used to reform diesel.

For effective ATR, catalytic heterogeneous reactions are preferred over non-catalytic homogeneous reactions. The activity and H_2 selectivity of the reforming catalysts are key points in estimating the performance. Several catalysts have been introduced for hydrocarbon reforming. Widely used transition metal-based catalysts, such as Ni and Co, have been investigated for effective hydrocarbon reforming [5,13,14]. But, it is still controversial whether they can be used as catalysts for diesel ATR, because of severe carbon deposition and sulfur poisoning [8]. Noble metal catalysts such as Pt, Rh, Ru, and Pd have shown higher performance than transition metals such a as Ni and Co [5,15,16]. A bimetallic catalyst of Pt–Pd showed higher performance than the catalyst using only Pt [17].

The role of substrates for supporting metal catalysts is very important. They are not merely a simple mechanical support, but also catalysts that participate in the heterogeneous reaction mechanism [16]. Fluorite and pervoskite-structured ceramic materials were introduced as representative substrates for higher chemical activity [18,19]. For example, CeO_2 is a widely used fluorite material with high oxygen storage capacity (OSC). As seen in Fig. 1, CeO_2 has a cubic structure with four Ce^{4+} ions and eight O^{2-} ions in a unit cell. Therefore, the CeO_2 structure is expressed as AO_2 (fluorite structure). If two A sites (Ce^{4+}) are substituted with two Ge^{3+} ions, one oxygen ion would be expelled due to the principle of charge neutrality. As a result, oxygen ion vacancies ($V_O^{\bullet\bullet}$) are generated. Oxygen vacancies ($V_O^{\bullet\bullet}$) and metal sites (M^0) on the surface of the substrates participate in the reforming process. O_2 is adsorbed on the catalyst surface and then O_{2ad} (and/or $2O_{ad}$) diffuse-out over the surface of catalyst [20]. When active metal sites are encountered, O_{ad} would go into the oxygen ion (O^{2-}) vacancies as expressed in the reaction below. This shows how to generate active oxygen ions from CeO_2. Oxygen goes in and out of the oxygen ion vacancies, which is linked with the reforming performance [21].

$$M^0 + 2V_O^{\bullet\bullet} + O_2 = M^{4+} + 2O^{2-}$$

Oxygen ion vacancies may also play an important role in the decomposition of water as expressed in the following reaction [21]:

$$M^0 + V_O^{\bullet\bullet} + H_2O = M^{2+} + O^{2-} + H_2$$

In this paper, other fluorite and perovskite-structured materials with OSC, such as yttrium (Y)-stabilized ZrO_2 (YSZ) and $Pr_{0.3}Sr_{0.7}CoO_3$ (PSC), were additionally investigated. Metal screening using the Gd-doped CeO_2 (CGO) substrate was also performed.

The performance of the reforming catalysts was evaluated by their H_2 production rate. The reforming activity can sometimes be very low, even with excellent catalysts, because of poor mixing problems in the case of diesel ATR. Unlike gas-phase lighter hydrocarbons, the reforming performance of heavier hydrocarbons, such as diesel, is seriously affected by the fuel delivery process [10,22]. It is hard to vaporize diesel due to its wide range of high boiling points. Ineffective vaporization brings inhomogeneous mixtures of diesel and oxidants (O_2 and/or H_2O) to the reactor entrance, which can influence the catalyst activity [10]. In order to enhance the mixing efficiency of diesel, it is usually injected into the combustion (or mixing) chamber by using a high-pressure injector (HPI). But it is slightly difficult to adapt the HPI to the diesel reformer, because injecting diesel at high pressure sometimes results in poor mixing as it comes into contact with the catalyst surface. This can result in excessively high

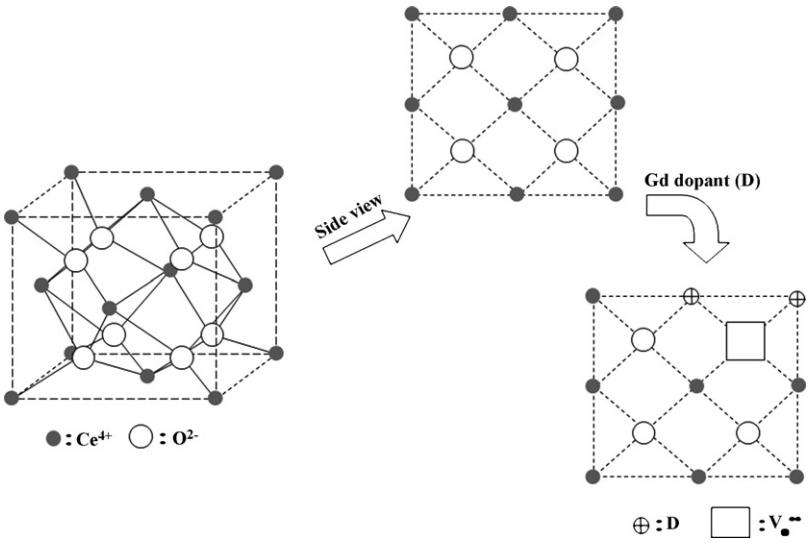

Fig. 1. Crystal structure of Gd 20 mol%-doped CeO_2 (CGO82).

temperatures that can damage or destroy the reforming catalyst [23].

In this paper, we have validated an ultrasonic injector (UI, US Patent pending: 11//549,359) and a plasma injector (PI) as effective diesel delivery systems. The UI can physically atomize diesel with mechanical force by a piezoelectric transducer. It requires lower power consumption than a typical heating-type vaporizer or a high-pressure nozzle-type injector. UI reforming showed 20% higher performance than non-UI reforming [10]. In this study, the long-term stability of the UI reformer was examined. On the other hand, a PI can lead to chemical excitation of the reactants as well as physical vaporization of diesel. The results of the PI reforming tests are presented as well.

2. Experimental

Micro-reactors for diesel ATR were prepared using 1/2 in. STS (stainless steel) tubes installed in an electrical furnace. Three pipelines were prepared for the delivery of the fuel, water, and air. In addition, a N_2 line was also installed to uniformly deliver the vaporized water. The fuel and water were delivered by HPLC (high-performance liquid chromatograph) pumps (MOLEH Co., Ltd.). Ultra pure water (>15 MΩ) was vaporized using an external heat exchanger. The flowrates of air and N_2 were controlled individually by mass flow controllers (MKS). The experimental setup was previously described in detail [9].

Catalysts were prepared using glycine nitrate process (GNP) and incipient wetness impregnation (IWI). Pt on Gd-doped CeO_2 (CGO–Pt) and $Pr_{0.3}Sr_{0.7}CoO_3$ were synthesized by the GNP. The nitrate precursors used to synthesize each catalyst are listed in Table 1. The precursors were dissolved in de-ionized water and after the water was boiled-off using a hot plate, green catalyst powders were obtained. Calcination of each catalyst was conducted at 900 °C for 4 h (CGO–Pt) and at 1200 °C for 1 h (PSC), respectively. After synthesis of CGO–Pt and PSC, their structure was identified by X-ray diffraction (XRD) measurements. They were in good agreement with the reference fluorite and perovskite-structured materials. Finally, the catalyst powders were pelletized using a uni-axial press and then crushed into granules of regular size (~500 μm).

On the other hand, Pt on Al_2O_3 (Al_2O_3–Pt) was prepared using the IWI process. Fine γ-Al_2O_3 (high purity chemicals) powder was fabricated into regular granules of ~500 μm. Then, a Pt nitrate solution was impregnated into the Al_2O_3 granule. A yttrium-stabilized ZrO_2 powder was supplied by TOSOH (TZ-8YS) and was also used as a granule type catalyst. All prepared catalysts were loaded inside the stainless steel tubes. Two k-type thermocouples were installed at the top and bottom of the catalyst bed to monitor the reaction temperatures.

Table 1
Nitrate precursors prepared for catalyst synthesis using GNP

Catalysts	Nitrate precursors	Supplier
CGO–Pt	Cerium (Ce): $Ce(NO_3)_3{\cdot}6H_2O$	Alfa Aesar
	Gadolinium (Gd): $Gd(NO_3)_3{\cdot}6H_2O$	Aldrich
	Platinum (Pt): $(NH_3)_4Pt(NO_3)_2$	Aldrich
	Glycine $C_2H_5NO_2$	Sigma
PSC	Praseodymium (Pr): $Pr(NO_3)_3{\cdot}6H_2O$	Sigma
	Strontium (Sr): $Sr(NO_3)_2{\cdot}6H_2O$	Sigma
	Cobalt (Co): $Co(NO_3)_2{\cdot}6H_2O$	Sigma
	Glycine: $C_2H_5NO_2$	Sigma

Table 2
Slurry composition for fabrication of microchannel catalysts

	Gravimetric ratio to catalyst powder	Supplier
Catalyst powder	1	Proxair
Organic solvent	4	Sigma–Aldrich
Dispersant	0.05	Sigma–Aldrich
Plasticizer	0.05	Sigma–Aldrich
Binder	0.04	Sigma–Aldrich

The microchannel catalysts were fabricated using Inconel625 (Ni 61/Cr 22/Mo 9/Fe 5) mesh. First, the mesh was oxidized in air at 950 °C for 6 h in order to form a thin oxide layer. It was then coated with CGO–Rh and CGO–Pt by the slurry dipping process and dried in an oven at 110 °C. The detailed slurry composition is listed in Table 2. Such slurry dipping of the metal mesh was performed six times. After it was wound, it was calcined at 900 °C for 26 h. The prepared microchannel catalysts are shown in Fig. 2.

Simulated sulfur free diesel (mixture of $C_{12}H_{26}$ and $C_{11}H_{10}$) and commercial diesel (GS-Caltex, Korea) were prepared as fuels for the diesel ATR experiments. The reforming performance of our simulated diesel was in good agreement with commercial diesel [24]. Using simulated diesel allows for easier calculation of the basic stoichiometries, such as O_2/C and H_2O/C, and the fuel conversion.

After moisture removal in the reformate, product gases were analyzed by a gas chromatograph (GC, Agilent 6890N) with a thermal conductivity detector (TCD) and a flame ionization detector (FID). The TCD, which uses argon (Ar) as the carrier gas, was used to analyze the relative amounts of H_2, CO, CO_2,

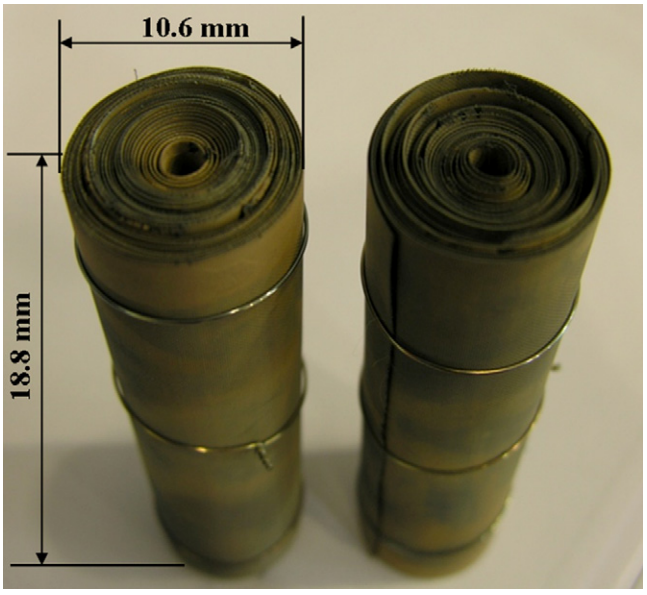

Fig. 2. Microchannel catalysts using Inconel mesh.

O_2, and N_2 and the FID which uses helium (He) as the carrier gas, was used to analyze the relative amounts of CH_4, C_2H_2, C_2H_4, C_2H_6, C_3H_6, C_3H_8, *iso*-C_4H_{10}, normal-C_4H_{10}, normal-C_5H_{12}, C_6H_{12} (cyclo-hexane), C_6H_6 (benzene), and *iso*-C_8H_{18}. Carbon deposits on the aged catalysts were analyzed using TGA/DSC (thermogravimetric analysis/differential scanning calorimetry) measurements.

The ultrasonic injector consists of a vibrating part, using a piezoelectric ceramic (PZT), and an injector cooling part. The performance and schematic design of the UI was previously introduced in detail [10]. A schematic design of the PI injector is described in Fig. 3(a). The plasma is generated between the end of an electrode and the body of the PI as shown in Fig. 3(b). The power consumption of the PI was about 300 W at normal conditions. Information about the PI was previously introduced in detail [25].

3. Results and discussion

3.1. The test of reforming catalysts

Gd 20 mol%-doped CeO_2 (CGO82) and Al_2O_3 substrates were prepared to validate the effect of the substrate on the reforming performance. Al_2O_3 is a widely used inert substrate with a high BET surface area. On the other hand, CGO82 has a BET surface area of ~35 m^2/g. Pt 0.5 wt.% on CGO82 (CGO82–Pt) and Pt 0.5 wt.% on Al_2O_3 (Al_2O_3–Pt) was prepared using GNP and IWI, respectively. From the data plotted in Fig. 4, H_2 yields obtained when using the substrates alone or a blank reactor were compared to distinguish the chemical activity of the substrates. In this paper, the labels of 'H_2 yield (mol/mol)' on *y*-axis in figures mean 'mol H_2 produced/mol hydrocarbon fed'. The H_2 produced from the Al_2O_3-packed reactor gives almost the same H_2 yield to that of the blank (no catalyst-packed) reactor. This shows that the Al_2O_3 has no catalytic activity. On the other hand, CGO82 shows relatively high H_2 yield as seen in Fig. 4. When Pt is added onto the Al_2O_3, Al_2O_3–Pt produces more H_2 than Al_2O_3 alone indicating that Pt plays a key role in H_2 generation. While CGO82–Pt shows slightly higher H_2 yields than CGO82 alone. Unlike Al_2O_3, CGO82 plays a chemically important role.

The high reforming performance of CGO82 is related to the characteristics of CeO_2, such as OSC. Reduction and oxidation (redox) through oxygen vacancies of CeO_2 may enhance the reforming performance. H_2 yields were investigated while increasing the amount of the Gd dopant to investigate whether or not oxygen vacancies actually increase the reforming performance. The reforming performances were compared between three samples: CeO_2 (no Gd dopant), Gd 10 mol%-doped CeO_2 (CGO91) and Gd 20 mol%-doped CeO_2 (CGO82). From the data plotted in Fig. 5, we can see that H_2 yields increased with an increasing amount of Gd. Increased Gd doping into CeO_2 would create more oxygen vacancies and would enhance the redox process in CeO_2.

We have investigated other materials with OSC, such as YSZ (fluorite structure) and PSC (pervoskite structure). These materials are used in SOFC technology. Practically, doped

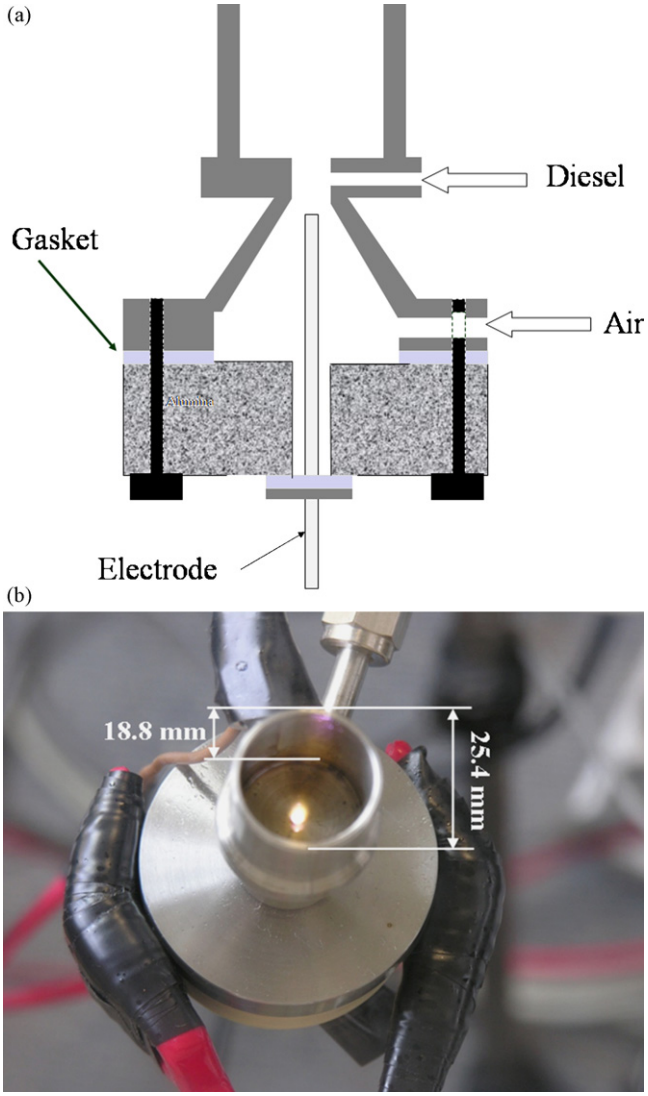

Fig. 3. Plasma injector (a: schematic design; b: plasma generation).

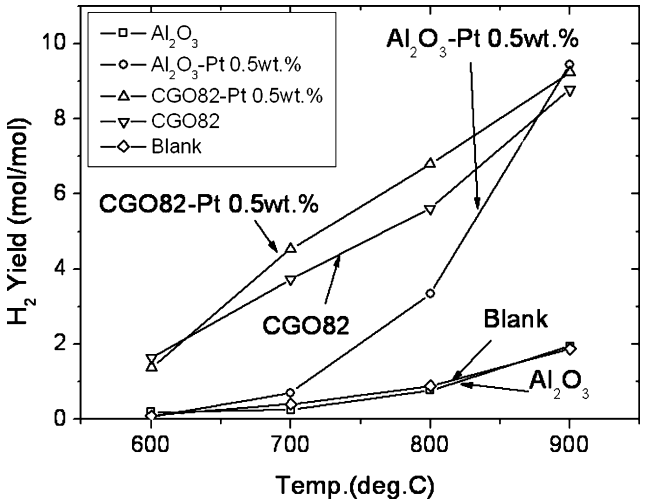

Fig. 4. H_2 yields of CGO82 (Pt 0.5 wt.%) and Al_2O_3 (Pt 0.5 wt.%) (synthetic diesel, O_2/C = 0.5, H_2O/C = 1.25, GHSV = 5000 h^{-1}).

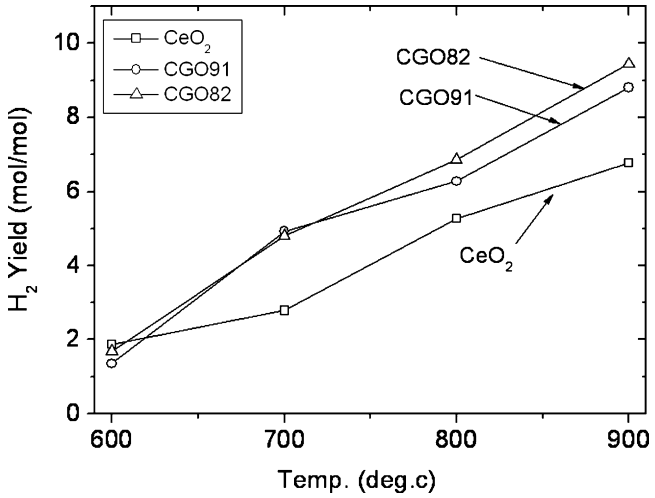

Fig. 5. Effect of Gd dopant in CeO_2 on H_2 yield (synthetic diesel, O_2/C = 0.5, H_2O/C = 1.25, GHSV = 5000 h^{-1}).

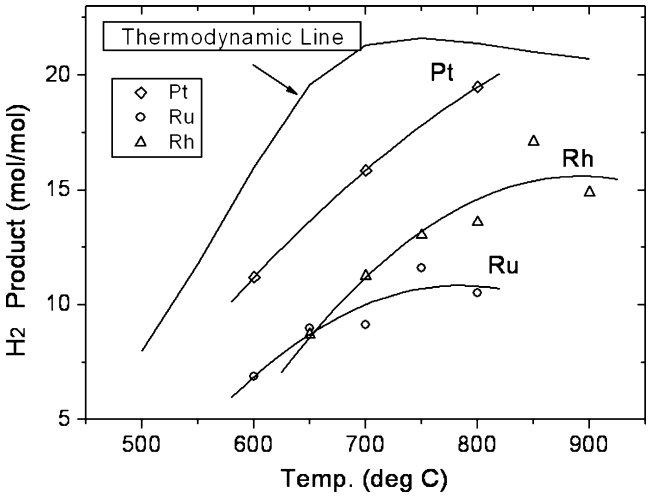

Fig. 7. Effect of metals (Pt: 0.5 wt.%; Rh: 0.5 wt.%; Ru: 0.5 wt.%) on H_2 yield [9] ($C_{16}H_{34}$, O_2/C = 0.5, H_2O/C = 1.25, GHSV = 5000 h^{-1}).

CeO_2 can be used as a low temperature-operating electrolyte in SOFC. YSZ (yttrium-stabilized ZrO_2) and PSC have similar properties as CeO_2. YSZ is the most representative ceramic material used as an electrolyte of SOFC and PSC is a candidate cathode material in SOFC with its mixed ionic and electronic conductivities (MIEC). From the data plotted in Fig. 6, YSZ and PSC also showed higher H_2 yields than Al_2O_3, although their performance was lower than CeO_2. But all substrates still have low H_2 yields compared to H_2 yield in thermodynamic equilibrium state.

The effect of metal catalysts (Pt, Rh, and Ru) have been already investigated using CGO82 as a substrate in previous work [9]. In Fig. 7, Pt produces higher H_2 yields than Rh and Ru. At 800 °C, H_2 yields approach thermodynamic equilibrium. With increasing amounts of Pt (= 0.5, 1, 2, and 3 wt.% of the substrate) in the CGO82, hydrogen yields increase as shown in Fig. 8. The catalysts have a large difference in performance between 700 and 800 °C as seen in Fig. 8. At 600 °C, H_2 yields were very low for all catalysts indicating that the catalysts were not activated. At 900 °C, most of the catalysts have similar H_2 yields because the reaction is more dependent on the operating temperature than the catalysts. In addition, we have tested the effect of a bimetallic catalyst. The behavior of CGO82–Pt and Ni 4 wt.%-impregnated CGO–Pt (CGO–PtNi) was compared and CGO–PtNi showed a greater reforming performance than CGO–Pt as seen in Fig. 9.

Carbon deposition on the catalyst needs to be minimized in order to obtain long-term performance of diesel ATR. Once carbon forms in the catalyst bed, it is difficult to remove it, reversibly. Carbon can deactivate the catalyst by blocking active sites. We measured the amount of carbon formed on three aged catalysts (Al_2O_3–Pt, CGO–Pt, and CGO–PtNi) after the reforming experiment using TGA/DSC. Fig. 10 shows the DSC results using oxygen for the aged catalysts. The aged Al_2O_3–Pt had a much larger amount of carbon than the other two catalysts. Carbon on Al_2O_3–Pt are burned at temperatures greater than 500 °C, which means that most of the carbon was generated by thermal pyrolysis at high temperatures [26]. On

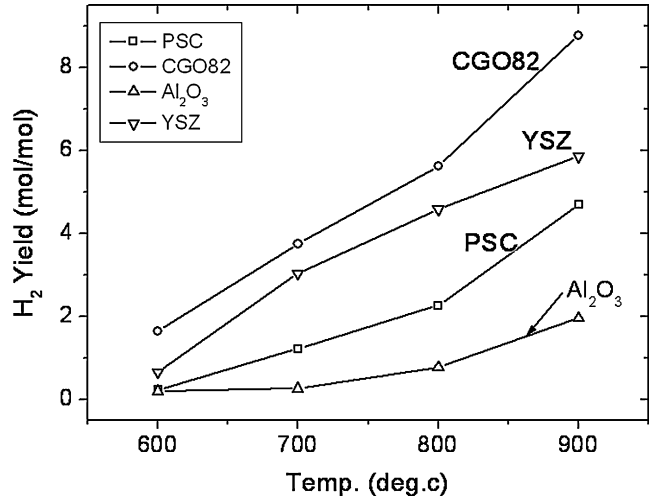

Fig. 6. H_2 yields of CGO82, YSZ, PSC and Al_2O_3 (synthetic diesel, O_2/C = 0.5, H_2O/C = 1.25, GHSV = 5000 h^{-1}).

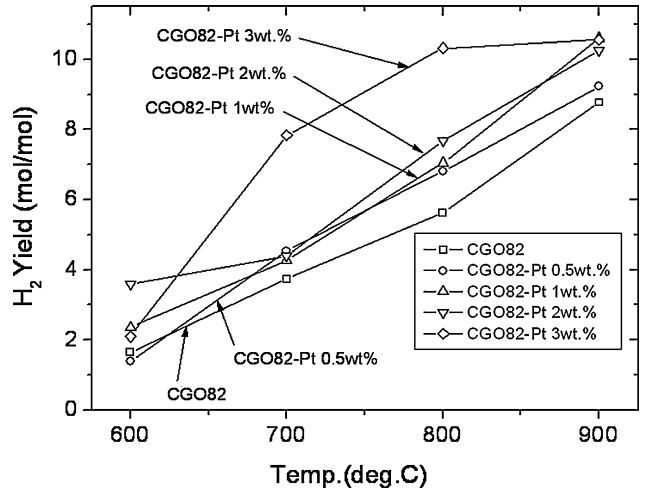

Fig. 8. Effect of the metal (Pt) content on H_2 yields (synthetic diesel, O_2/C = 0.5, H_2O/C = 1.25, GHSV = 5000 h^{-1}).

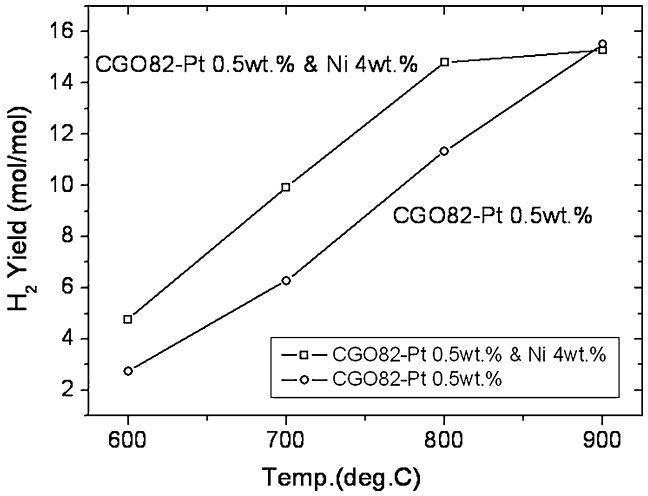

Fig. 9. H_2 yields of CGO82–Pt 0.5 wt.% vs. CGO82–Pt 0.5 wt.%–Ni 4 wt.% (synthetic diesel, O_2/C = 0.5, H_2O/C = 1.25, GHSV = 5000 h^{-1}).

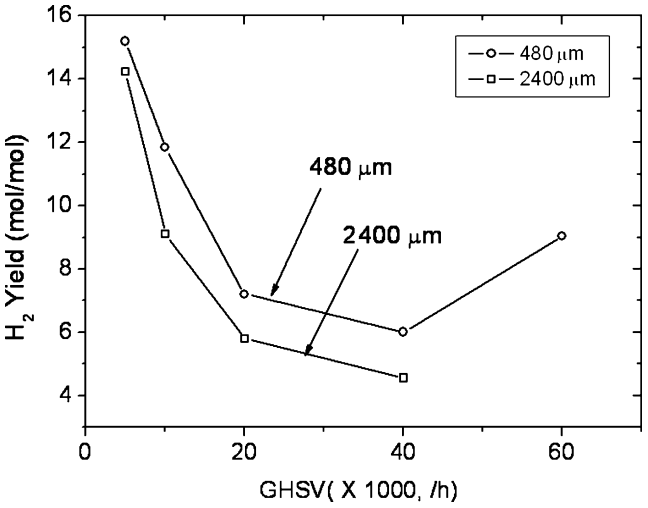

Fig. 11. H_2 yields using different catalysts in size with respect to GHSV (synthetic diesel, O_2/C = 0.5, H_2O/C = 1.25, temperature = 800 °C).

the other hand, CGO–Pt and CGO–PtNi have carbons peaks near 400 °C because the carbon was generated by CH_x polymerization and (/or) CH_4 decomposition [26]. Interestingly, CGO–PtNi had greater amounts of carbon deposition than CGO–Pt although it had higher H_2 yields.

After the reforming catalyst materials are chosen, the effect of particle geometry (shape) needs to be considered. Generally, a packed bed of a pellet-typed catalyst is used to test the performance of the catalyst due to its easy fabrication. The reforming test is usually performed at very low gas flowrates in order to exclude mass transfer limitations. Fig. 11 shows H_2 yields with GHSV (gas hourly space velocity) using different granule size (~480 μm and ~2400 μm) CGO–Pt catalysts. The reforming performance clearly decreased with increasing GHSV. The ~2400 μm-size catalyst showed a much larger decrease in H_2 yield than the ~480 μm-size granules. Although the particle size needs to be increased in order to decrease the pressure drop of the catalyst bed at high gas flowrates, a larger particle size results in the decrease of open surface of the catalysts under the fixed bed volume and decreases the particle effectiveness factor [27]. The performance of larger particles show greater degradation compared to smaller particles as seen in Fig. 11. This type of catalyst bed is not efficient in the engineering of a reactor driven at high gas flowrates.

Microchannel typed catalysts using metal mesh have been fabricated as shown in Fig. 2. From the data plotted in Figs. 12 and 13, we can see the product distribution with GHSV. In these figures, the labels of 'Product (mol/mol)' on *Y*-axis mean 'mol product/mol hydrocarbon fed'. And the efficiency plotted in figures of this paper is defined by (LHV of H_2 produced + LHV of CO produced)/(LHV of the fuel used). In Fig. 12, the reforming performance is maintained until 50,000 h^{-1}. On the contrary, H_2 yields slightly increase at 10,000–40,000 h^{-1} compared to 5000 h^{-1}. But, the probability of carbon deposition increases with increasing GHSV. In Fig. 13, C_2H_4, a representative carbon precursor [12,28], increases with respect to GHSV because of poor mixing of the fuel at high gas flowrates. The reformate was anal yzed as the function of operating time using CGO–Pt 2 wt.%

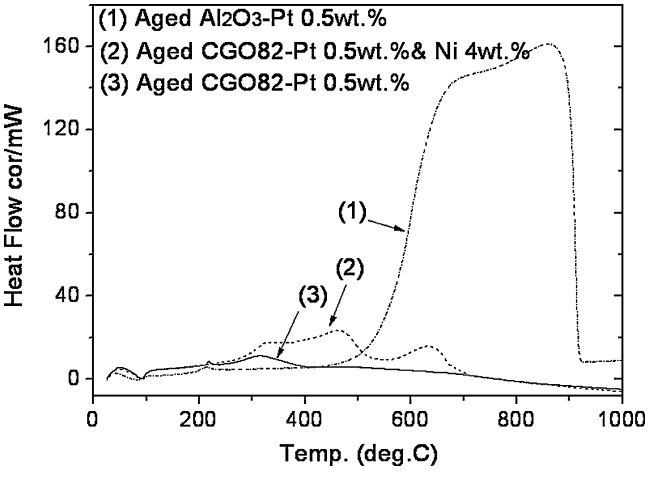

Fig. 10. DSC measurement of aged catalysts (Al_2O_3–Pt, CGO82–Pt, and CGO82–PtNi) (DSC: differential scanning calorimetry).

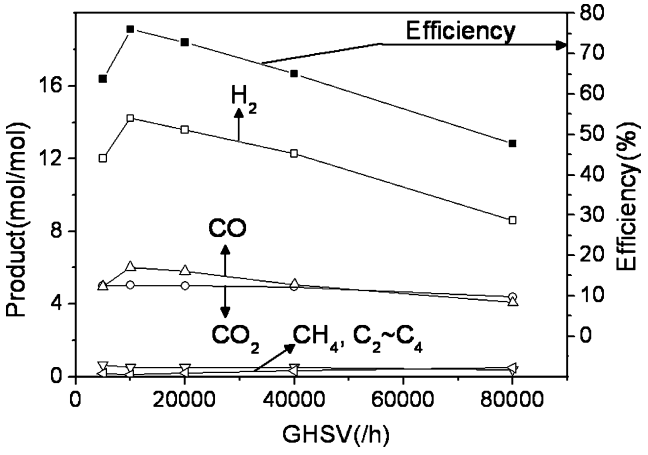

Fig. 12. Reforming efficiency (RE) and product distribution of Rh-microchannel catalyst with respect to GHSV (synthetic diesel, O_2/C = 0.5, H_2O/C = 1.25, temperature = 800 °C, CGO82–Rh 0.5 wt.%, RE = LHV ratio of H_2 + CO and fuel).

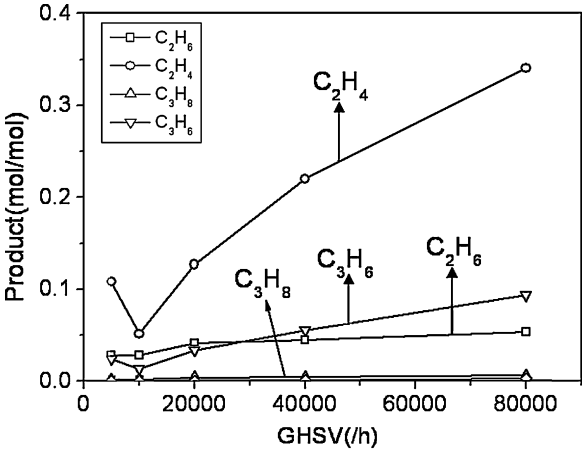

Fig. 13. Lighter hydrocarbon distribution of Rh-microchannel catalyst with respect to GHSV (synthetic diesel, $O_2/C = 0.5$, $H_2O/C = 1.25$, temperature = 800 °C, CGO82–Rh 0.5 wt.%).

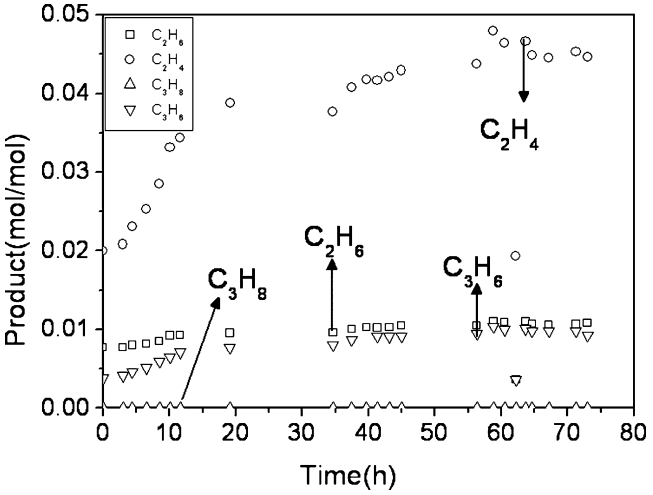

Fig. 15. Lighter hydrocarbon distribution of Pt-microchannel catalyst with respect to operating time (synthetic diesel, $O_2/C = 0.8$, $H_2O/C = 2$, temperature = 800 °C, CGO82–Pt 2 wt.%, GHSV = 30,000 h^{-1}).

on a metal mesh. The reforming performance showed little degradation for about 75 h as seen in Fig. 14. But, the carbon precursor, C_2H_4, doubled when compared to the initial time as seen in Fig. 15. The increase in C_2H_4 is not related to catalyst, but the fuel delivery process. This will be discussed in the next section.

3.2. Fuel delivery apparatuses

C_2H_4 is a dominant carbon precursor. In this study, it was found that C_2H_4 is not generated over the catalyst surface, but produced by thermal pyrolysis of long-chain hydrocarbons at the reactor entrance before reaching catalyst bed [12]. Greater amounts of C_2H_4 were generated if a homogeneous fuel mixture with oxidants was not attained, eventually leading to severe carbon deposition on the catalyst surface. Therefore, in order to improve the reforming performance, an effective fuel delivery system has to be considered with catalyst development.

It is difficult to vaporize diesel due to its wide range of high boiling points. Ineffective vaporization brings an inhomogeneous mixture of diesel with oxidants (O_2 and/or H_2O) to the reactor entrance, which can influence the reforming performance [10]. In diesel-related industries, diesel is usually delivered into the combustion (or mixing) chamber by using a high-pressure injector to enhance the mixing between the reactants. But, due to several disadvantages of the HPI in a diesel reformer, an ultrasonic injector (US Patent pending: 11// 549,359) was used instead. The UI reforming was very effective. Reforming efficiencies increased as much as 20% compared to non-UI reforming [10]. In this study, we investigated the long-term durability of the UI reformer. In the case of the non-UI reformer, the reforming performance slightly decreased, as shown in Fig. 16. The amount of C_2H_4 formed clearly increases at 150 h as seen in Fig. 17. On the other hand, the UI reformer has very stable performance as seen in Fig. 18. From the data plotted in Fig. 19, we can see that C_2H_4 formation is very well controlled. C_2H_4 formation in the UI reforming is one order of magnitude less than the non-UI

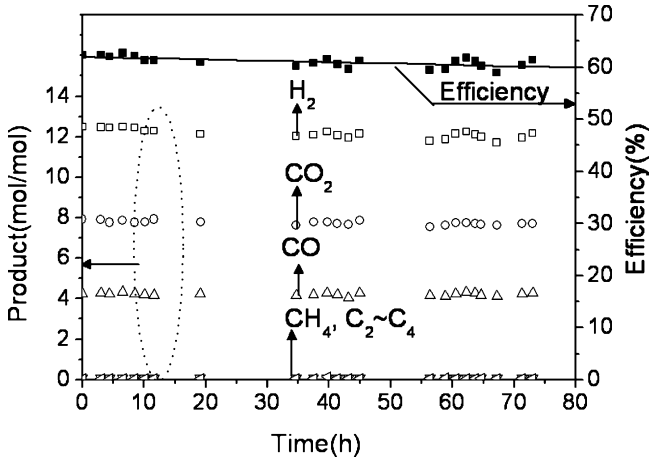

Fig. 14. Reforming efficiency and product distribution of Pt-microchannel catalyst with respect to operating time (synthetic diesel, $O_2/C = 0.8$, $H_2O/C = 2$, temperature = 800 °C, CGO82–Pt 2 wt.%, GHSV = 30,000 h^{-1}).

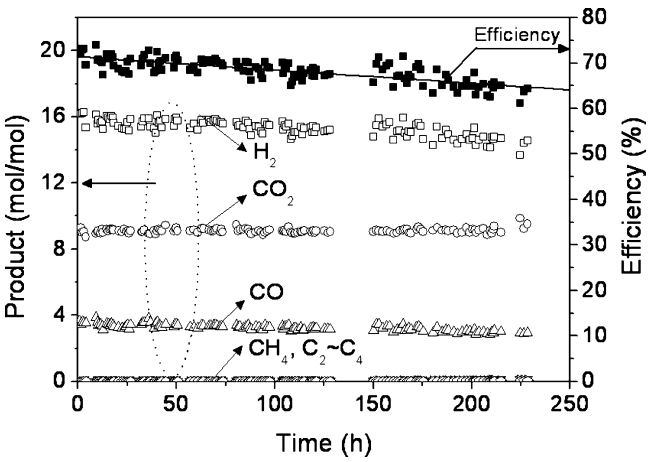

Fig. 16. Product distribution in non-UI reforming with respect to operating time (synthetic diesel, $O_2/C = 0.8$, $H_2O/C = 3$, temperature = 800 °C, GHSV = 12,500 h^{-1}, CGO–Pt 0.5 wt.%, no ultrasonic injector).

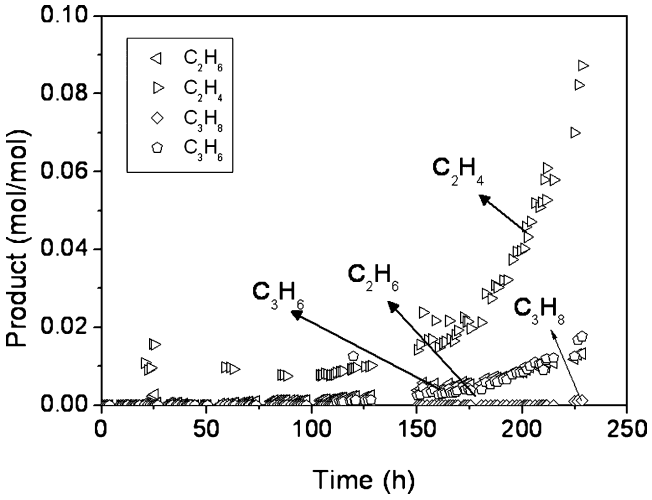

Fig. 17. Lighter hydrocarbon distribution in non-UI reforming with respect to operating time (synthetic diesel, O_2/C = 0.8, H_2O/C = 3, temperature = 800 °C, GHSV = 12,500 h^{-1}, CGO–Pt 0.5 wt.%, no ultrasonic injector).

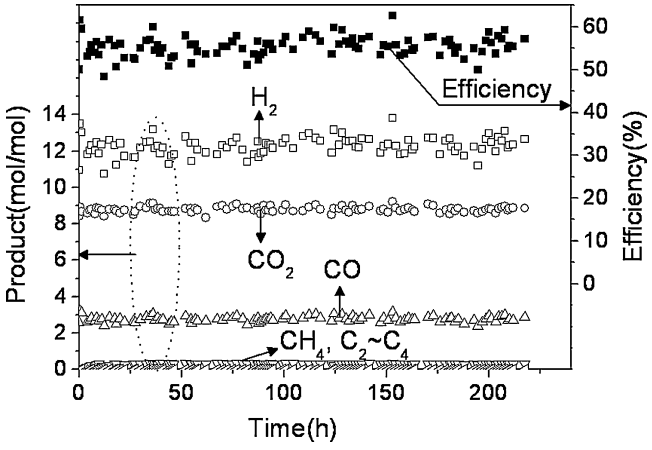

Fig. 18. Reforming efficiency and product distribution in UI-reforming with respect to operating time (synthetic diesel, O_2/C = 0.8, H_2O/C = 3, temperature = 800 °C, GHSV = 12,500 h^{-1}, CGO–Pt 0.5 wt.%, ultrasonic injector usage).

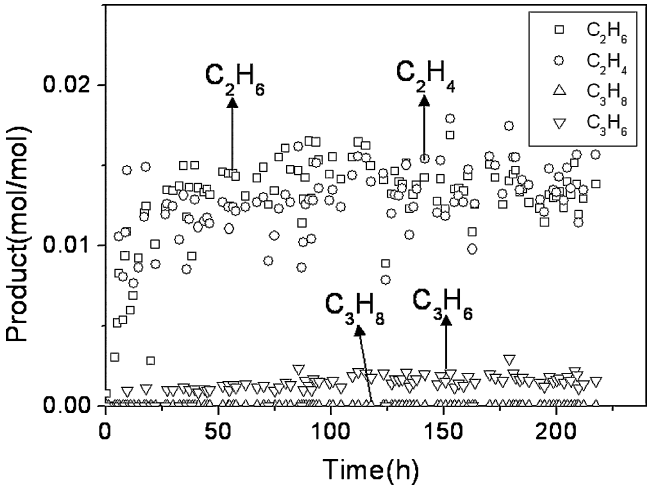

Fig. 19. Lighter hydrocarbon distribution in UI-reforming with respect to operating time (synthetic diesel, O_2/C = 0.8, H_2O/C = 3, temperature = 800 °C, GHSV = 12,500 h^{-1}, CGO–Pt 0.5 wt.%, ultrasonic injector usage).

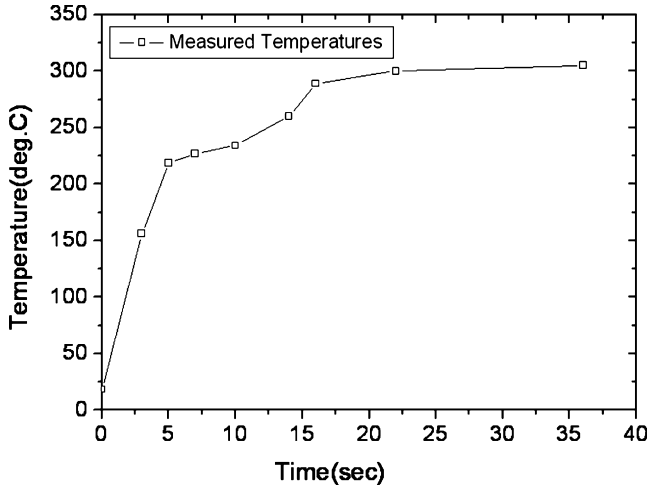

Fig. 20. Temperature profile during start-up of PI-reforming (the measure point: ~1 mm distance of injection hole, air = 2486 ml/min).

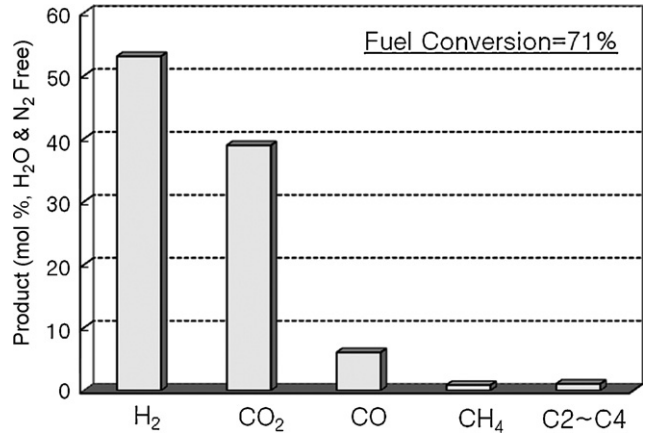

Fig. 21. Product distribution in PI-reforming (commercial diesel, O_2/C = 0.56, H_2O/C = 1.25, GHSV = 12,500 h^{-1}, CGO–Pt).

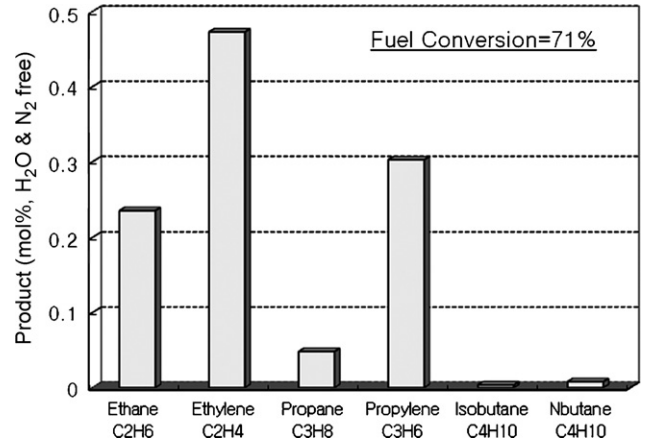

Fig. 22. Lighter hydrocarbon distribution in PI-reforming (commercial diesel, O_2/C = 0.56, H_2O/C = 1.25, GHSV = 12,500 h^{-1}, CGO–Pt).

reforming. The UI would be a good candidating technology for fuel delivery system of the diesel reformer.

Unlike the UI, which can physically atomize diesel, a plasma injector, which can physically and chemically atomize diesel, has been investigated. Although the PI causes the light-off time of the fuel to be very short (∼20 s, considering the light-off temperature of diesel is about 300 °C [29]), as shown in Fig. 20, the reforming performance is not satisfactory. The product distribution from PI reforming is shown in Figs. 21 and 22. In Fig. 21, H_2 yields have relatively high values. The fuel conversion had low value of 71% compared to ∼100% fuel conversion in UI reforming. The fuel conversion was defined by (carbons of CO, CO_2 and CH_4 in product)/(carbons of fuel used). In addition, C_2H_4 has the very large portion of the unreacted hydrocarbons as seen in Fig. 22. The PI reformer was actually shut-off after 4 h of operation due to severe carbon deposition. Elaborate control of the PI would be required.

4. Conclusions

In diesel reforming, both the reforming catalysts and the fuel delivery systems are very important. Pt on Gd-doped CeO_2 showed better performance than other selected catalysts. The CGO substrate takes a chemical role in producing hydrogen as well as a mechanical role in supporting metal catalysts. CGO also exhibited an excellent ability to suppress carbon deposition on the catalyst surface. With catalyst selection, fuel delivery systems have to be designed for effective fuel delivery to form homogeneous mixtures of the fuel and oxidants, which would suppress the generation of carbon precursors, such as C_2H_4, by thermal pyrolysis of heavier hydrocarbons. The UI is an excellent candidate system considering these aspects. It shows very stable performance as a function of time. On the other hand, further study of the PI is required with efforts to suppress carbon deposition. Ultimately the diesel reformer that we have mentioned so far would be used as a feeding system for SOFC. For extending the life time of SOFC systems, the performance such as high fuel conversion and high H_2 selectivity should be obtained.

Acknowledgements

This work was performed from the projects funded by the Korean Government, ‘‘Zero Emission Vehicle project’’ with the Korea Institute of Machinery and Materials (KIMM), ‘‘5 kW_e Diesel-driven SOFC System’’ with the Korea Electric Power Research Institute (KEPRI) and ‘‘the fostering project of the Best Lab’’ with the Ministry of Commerce, Industry and Energy (MOCIE).

References

[1] C. Song, Catal. Today 77 (2002) 17.
[2] D.-J. Liu, T.D. Kan, H.-K. Liao, S. Ahmed, Int. J. Hydrogen Energy 29 (2004) 1035‘.
[3] S. Ahmed, M. Krumpelt, Int. J. Hydrogen Energy 26 (2001) 291.
[4] A. Heinzel, B. Vogel, P. Hübner, J. Power Sources 105 (2002) 202.
[5] S. Ayabe, H. Omoto, T. Utaka, R. Kikuchi, K. Sasaki, Y. Teraoka, K. Eguchi, Appl. Catal. A 241 (2003) 261.
[6] S.H.D. Lee, D.V. Applegate, S. Ahmed, S.G. Calderone, T.L. Harvey, Int. J. Hydrogen Energy 30 (2005) 829.
[7] J. Park, Numerical Investigation of Steam Reformer for Fuel Cells, Master’s Thesis, KAIST, Deajeon, 2007, Chapter 4, p. 68.
[8] S.K. Goud, W.A. Whittenberger, S. Chattopadhyay, M.A. Abraham, Int. J. Hydrogen Energy 32 (2007) 2868.
[9] I. Kang, J. Bae, J. Power Sources 159 (2006) 1283.
[10] I. Kang, J. Bae, S. Yoon, Y. Yoo, J. Power Sources 172 (2007) 845.
[11] P.K. Cheekatamarla, A.M. Lane, J. Power Sources 152 (2005) 256.
[12] S. Yoon, I. Kang, J. Bae, J. Korean Elec. Soc. 10 (2007) 110.
[13] Y.-S. Oh, H.-S. Roh, K.-W. Jun, Y.-S. Baek, Int. J. Hydrogen Energy 28 (2003) 1387.
[14] M.S. Batista, R.K.S. Santos, E.M. Assaf, J.M. Assaf, E.A. Ticianelli, J. Power Sources 124 (2003) 99.
[15] M. Krumpelt, T.R. Krause, J.D. Carter, J.P. Kopasz, S. Ahmed, Catal. Today 77 (2002) 3.
[16] D. Duprez, Catal. Today 112 (2006) 17.
[17] P.K. Cheekatamarla, A.M. Lane, Int. J. Hydrogen Energy 30 (2005) 1277.
[18] M. Krumpelt, J.D. Carter, R. Wilkenhoener, S.H.D. Lee, J.-M. Bae, S. Ahmed, in: Proceedings of the Fuel Cell Seminar, Portland, Oregon, October, (2000), p. 542.
[19] T. Krause, D. Carter, J.-M. Bae, S. Ahmed, M. Krumpelt, in: Proceedings of the 4th Wor. Cong. on Oxidation Catalysis, Germany, September 16–21, (2001), p. 138.
[20] E. Ivers-Tiffee, A. Weber, H. Schichlein, Handbook of Fuel Cells, vol. 2, Johne Wiley & Sons Ltd., England, 2003 (Chapter 40, p. 587).
[21] M. Krumpelt, T. Krause, J.D. Carter, J. Mawdsley, J.-M. Bae, S. Ahmed, C. Rossignol, Annual Progress Report, U.S. DOE, 2001, p.90.
[22] L. Hartmann, K. Lucka, H. Köhne, J. Power Sources 118 (2003) 286.
[23] T.R. Krause, S. Ahmed, R. Kumar, Proceedings of the 4th International Conference on Fuel Cell Science, Eng. and Tech., California, June 19–21, 2006, paper no. FUELCELL2006-97260.
[24] I. Kang, J. Bae, G. Bae, J. Power Sources 163 (2006) 538.
[25] D.H. Lee, K.T. Kim, N.K. Hwang, Y.H. Song, Proceedings of the 18th International Symposium on Transport Phenomena, Deajeon, August 27–30, 2007, paper no. 393.
[26] C.N. Satterfield, Heterogeneous Catalysis in Industrial Practice, 2nd ed., McGraw-Hill Inc., New York, 1993 (Chapters 6 and 10).
[27] R.W. Missen, C.A. Mims, B.A. Saville, Introduction to Chemical Reaction Engineering and Kinetics, John Wiley & Sons Inc., New York, 1999, p. 201.
[28] J.R. Rostrup-Nielsen, T.S. Christensen, I. Dybkjaer, Stud. Surf. Sci. Catal. 113 (1998) 81.
[29] R.L. Borup, M.A. Inbody, T.A. Semelsberger, J.I. Tafoya, D.R. Guidry, Catal. Today 99 (2005) 263–270.